Supplementary Information

Enhancement of Oxygen Reduction Reactivity on TiN by Tuning the Work Function *via* Metal Doping

Mitsuharu Chisaka,[*a] *Toshiyuki Abe,*[b] *Rong Xiang,*[c,d] *Shigeo Maruyama*[d] *and Hirofumi Daiguji*[d]

[a]Department of Sustainable Energy, Hirosaki University,

3 Bunkyo-cho, Hirosaki, Aomori 036-8561, Japan

[b]Department of Frontier Materials Chemistry, Graduate School of Science and Technology, Hirosaki University, 3 Bunkyo-cho, Hirosaki 036-8561, Japan.

[c]State Key Laboratory of Fluid Power and Mechatronic Systems, School of Mechanical Engineering,

Zhejiang University, Hangzhou 310027, China.

[d]Department of Mechanical Engineering, The University of Tokyo, 7-3-1 Hongo, Bunkyo-ku, Tokyo 113–8656, Japan.

*Author to whom correspondence should be addressed.

Phone/Fax: +81 172 39 3559; E-mail: chisaka@hirosaki-u.ac.jp (M. Chisaka)

S1. Experimental details.

Catalyst synthesis: The $Ti_{0.8}M_{0.2}O_xN_y$ catalysts were synthesised using a modified combustion method[S1–S3] without the use of supports. First, titanium oxysulfate powder (0.49 g, $TiOSO_4 \cdot nH_2O$; $n \fallingdotseq 1 \sim 2$, Kishida Chemical Co. Ltd., Osaka, Osaka, Japan) was dispersed in distilled water (371 cm^3) by stirring at room temperature in a polytetrafluoroethylene (PTFE) beaker containing a PTFE-coated magnetic stirrer bar. The outside bottom of the beaker was coated with a PTFE-carbon composite to facilitate heating on a hot stirrer. Then, one of the metal precursor powders, *i.e.*, zirconium chloride ($ZrCl_4$, Fuji Film Wako Pure Chemical Co., Osaka, Osaka, Japan) or niobium chloride ($NbCl_5$, Fuji Film Wako Pure Chemical Co., Osaka, Osaka, Japan) or nickel acetate tetrahydrate ($(CH_3COO)_2Ni \cdot 4H_2O$, Fuji Film Wako Pure Chemical Co., Osaka, Osaka, Japan), was added with continuous stirring. When preparing $Ti_{0.8}V_{0.2}O_xN_y$ catalysts, vanadium oxide powders (V_2O_5, Fuji Film Wako Pure Chemical Co., Osaka, Osaka, Japan) were dissolved in a 35% w/w solution of hydrochloric acid (36 cm^3, HCl, Kishida Chemical Co. Ltd., Osaka, Osaka, Japan), which was then added to the $TiOSO_4$ dispersion prepared as mentioned above, except that the volume of water was decreased to 335 cm^3. The atomic ratio of metal dopant to titanium was kept at 1 : 4 and the volume of the dispersion was kept at 371 cm^3. For investigating the effect of metal composition on the activity of niobium-doped catalyst series, the atomic ratio of Nb to Ti was varied from 1 : 9 to 3 : 7. Next, urea powder (20 g, $(NH_2)_2CO$, Wako Pure Chemical Co., Osaka, Osaka, Japan) was added to set the mass ratio of urea to $TiOSO_4$-derived TiO_2 to 100 and then a 35% w/w solution of HCl (36 cm^3, Kishida Chemical Co. Ltd., Osaka, Osaka, Japan) was added to the dispersion with continuous stirring. After this, the PTFE beaker was placed on a stirrer pre-heated to 523 K, stirred continuously until the water evaporated, and then further dried in a convection oven overnight at 380 K. The obtained dried powders were then ground using an agate mortar, placed in an alumina boat and the boat was set in a horizontal quartz-tube furnace. The tube was slowly evacuated, purged with N_2 gas, and the powder samples were heated from room temperature to various temperatures at a rate of 10 K min^{-1}, then the temperature was maintained for 2 h. Thereafter, the samples were cooled to room temperature at an

uncontrolled rate. The N_2 flow rate was 0.1 dm^3 min^{-1} during pyrolysis. After pyrolysis, the powders were ground in an agate mortar. Some solid by-products were noted to attach to the inner wall of the quartz tube during pyrolysis. These solid by-products present the danger of increasing the inner pressure of the tube by stopping the gas flow if they block the narrow opening of the quartz tube. To avoid such a situation, a quartz tube of more than three times longer than the heating zone was used to provide sufficient space for by-product accumulation inside the tube, thus ensuring that the gas flow was not blocked. After the pyrolysis, the tube was washed with water and heated at 1300 K for 2 h in air without any samples to completely remove the by-products.

Characterisation: The metal compositions of some $Ti_{0.8}M_{0.2}O_xN_y$ catalysts were evaluated using an energy dispersive X-ray spectrometer (JED-2300F, JEOL, Inc., Akishima, Tokyo, Japan). The measured atomic fraction of M was 0.19 ± 0.01, 0.23 ± 0.02, 0.24 ± 0.00 for M = Zr, Nb and Ni, respectively, thus all values were in good agreement with the nominal value of 0.2. As the characteristic X-ray energy from V Kα, 4.95 keV, is too close to that from Ti Kβ, 4.93 keV, and thus overlapping occurs, the vanadium composition of the $Ti_{0.8}V_{0.2}O_xN_y$ catalysts could not be evaluated. The morphology of the $Ti_{0.8}M_{0.2}O_xN_y$ catalysts was investigated using a field emission scanning electron microscope (JSM-7000F, JEOL Ltd., Akishima, Tokyo, Japan). The bulk crystal structures of the catalysts were analysed using an X-ray diffractometer (MiniFlex 600, Rigaku Co., Akishima, Tokyo, Japan) with Cu Kα radiation generated at 40 kV and 15 mA (scan range = 20–80°, step size = 0.02°, and scan rate = 2° min^{-1}). The crystal structures of the outermost surface were evaluated using an ultraviolet (UV)-Raman spectrometer (LabRAM HR-evolution, Horiba Scientific Co. Ltd., Kyoto, Kyoto, Japan) equipped with a 325 nm laser. The work function, Φ, of the $Ti_{0.8}M_{0.2}O_xN_y$ catalysts was evaluated using a photoemission yield spectrometer (AC-2S, Riken Keiki Co. Ltd., Itabashi, Tokyo, Japan) in air. The chemical states of the catalysts were determined using an X-ray photoelectron spectrometer (XPS, PHI 5000 VersaProbe, ULVAC-PHI, Inc., Chigasaki, Kanagawa, Japan) with an Al Kα X-ray source (1486.6 eV). The peak shifts due to surface charge were corrected using the binding energy of C 1s (284.8 eV) of the hydrocarbon

contaminants from the spectrometer and air. All the contaminants, surface TiO_2 layers and MO_x phases could contribute to O 1s spectra of the $Ti_{0.8}M_{0.2}O_xN_y$ catalysts in a manner that prevents them from being distinguished from one other. Therefore, the O 1s spectra were not analysed in this work. Instead, the *y* values of the $Ti_{0.8}M_{0.2}O_xN_y$ catalysts were determined after fitting the N 1s spectra with four symmetric peaks, as shown in Fig. S1. The peaks at ~369, ~397, ~399 and ~401 eV were labelled as N1, N2, N3 and N4 peaks, respectively. The N1 and N2–N4 peaks were assigned to nitrogen atoms in metal nitride and metal oxide, respectively.[S1–S5] As the surface nitrogen atoms in metal oxides are important for the oxygen reduction reaction (ORR)[S1,S2] and the surface of $Ti_{0.8}M_{0.2}O_xN_y$ catalysts was mostly amorphous oxide from the UV Raman spectra, shown in Fig. 1(b), the *y* values were calculated from the atomic ratio of the nitrogen of the N2–N4 peaks to the metals, (Ti + M) after subtracting a Shirley-type background. The spectra were acquired at least three different points for all the catalysts.

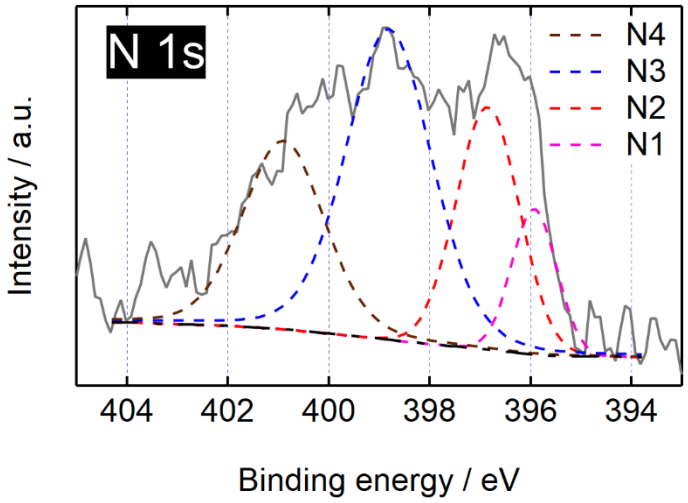

Fig. S1 X-ray photoelectron N 1s spectrum (solid curve) of a $Ti_{0.8}Zr_{0.2}O_xN_y$ catalyst after N_2-pyrolysis at 1123 K for 2 h with deconvolution into four peaks (dashed lines) after subtracting a Shirley-type background (dash-dotted line).

ORR activity and selectivity measurements: Rotating disk electrode (RDE) and rotating ring-disk electrode (RRDE) voltammograms were obtained to evaluate the ORR activity and selectivity,

respectively, of the catalysts. The catalyst, 5% w/w Nafion® ionomer solution (510211, Sigma-Aldrich Co., St. Louis, Missouri, U.S.) and isopropyl alcohol were sonicated together for 1200 s and then further mixed using a planetary mixer (Mazeru Star KK-250S, Kurabo Co., Osaka, Osaka, Japan) for 180 s to obtain a homogeneous catalyst ink. The mass fraction of Nafion in the catalyst layer was set at 0.05. The catalyst loading was set to be constant at 0.86 mg cm^{-2} by dropping 6.4 mm^3 of the catalyst ink onto a glassy carbon (GC) disk (4 mm diameter)–platinum ring (5 mm inner diameter and 7 mm outer diameter) electrode (012613, BAS Co., Sumida-ku, Tokyo, Japan). Prior to the treatment, the surface of the GC disk electrode was polished using 1.0 and 0.05 μm alumina slurries, cleaned with distilled water, ethanol, and then air-dried at 320 K for at least 600 s. A conventional three-electrode cell was used for the room-temperature electrochemical measurements performed in 0.1 mol dm^{-3} H_2SO_4. The catalyst-coated GC disk–Pt ring electrode, a carbon rod (diameter: 5 mm, C-072591, Nilaco Co., Chuo-ku, Tokyo, Japan), and Ag/AgCl (3 M NaCl) or Ag/AgCl (sat. KCl) electrode (RE-1B or RE-1CP, BAS Co., Sumida-ku, Tokyo, Japan) were used as the working, counter, and reference electrodes, respectively. The working electrode was set on a rotator (RRDE-3A, BAS Co., Sumida-ku, Tokyo, Japan). All working electrode potentials were referenced to the RHE. After sequentially bubbling O_2 and N_2 through 0.1 mol dm^{-3} H_2SO_4 for 1800 s, the RDE and RRDE voltammograms were recorded by applying a disk potential, E_d, of 0.05–1.2 V at a scan rate of 5 mV s^{-1} and a rotation speed of 1500 rpm, using a bipotentiostat (Model 2323 or 700B or 704B, BAS Co., Sumida-ku, Tokyo, Japan). The ring potential was maintained at 1.2 V to obtain the RRDE voltammograms. The ORR was measured according to $j = j_O - j_N$, the difference between the current per unit geometrical area, S, of the GC disk electrode obtained in N_2 ($j_N = I_N S^{-1}$) and in O_2 ($j_O = I_O S^{-1}$). The number of electrons transferred per unit oxygen molecule, n, values were calculated by analysing the RRDE voltammograms according to the following equation:

$$n = \frac{-I_d}{-I_d + I_r/N} \quad \text{(S1)}$$

where I_d and I_r denote the disk and ring currents, respectively, after the background correction described above, and N is the collection efficiency (0.424) provided by the manufacturer (BAS Co.). The kinetically controlled current density, j_k, was calculated using the following equation:

$$j_k = |j| \cdot |j_l| / (|j_l| - |j|) \quad \text{(S2)}$$

where j is the background corrected disk current density as mentioned above and j_l is the limiting current density.

The Nyquist plots were obtained by applying a root mean square alternating current voltage at 5 mV in the frequency range from 0.1 to 1.0 MHz at 0.7 V *versus* the RHE in O_2-saturated 0.1 mol dm^{-3} H_2SO_4 solution using a potentiostat equipped with a frequency response analyser (SP-150, Bio-Logic Science Instruments, Seyssinet-Pariset, Isère, France). The ohmic resistance of the measurement system, R, was determined from the high-frequency intercept of the Nyquist plots then all E_d values were corrected with R using the following equation:

$$E = E_d + |I_d|R \quad \text{(S3)}$$

The n and j_k values were evaluated at E = 0.6 and 0.7 V, respectively. The n–E curves of $Ti_{0.8}M_{0.2}O_xN_y$ catalysts are shown in Fig. S2.

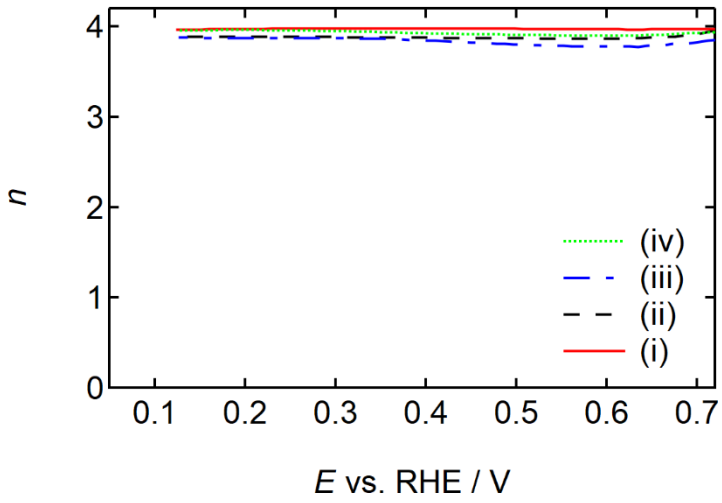

Fig. S2 The number of electrons transferred per unit oxygen molecule versus potential (*n*–*E*) curves of $Ti_{0.8}M_{0.2}O_xN_y$ catalysts, where M = (i) Zr, (ii) Nb, (iii) Ni and (iv) V.

S2. Crystal structures of the $Ti_{0.8}M_{0.2}O_xN_y$ catalysts.

The XRD patterns of the $Ti_{0.8}M_{0.2}O_xN_y$ catalysts around the TiN (2 0 0) plane are shown in Fig. S3. As mentioned in the main body of the text, some Zr, Nb and V ions were dissolved into the TiN lattice considering the ionic radii of these dopants and peak shifts observed from Fig. S2. The Φ values of the $Ti_{0.8}M_{0.2}O_xN_y$ catalysts measured in this work are 4.98 eV, 5.12 eV, 4.87 eV and 4.90 eV when M is Zr, Nb, Ni and V, respectively. The observed value trends are not dependent on the Φ values of polycrystalline Zr, Nb, Ni and V, which are 4.05 eV, 4.3 eV, 5.15 eV and 4.3 eV, respectively,[S6] thus ruling out the presence of segregated metal.

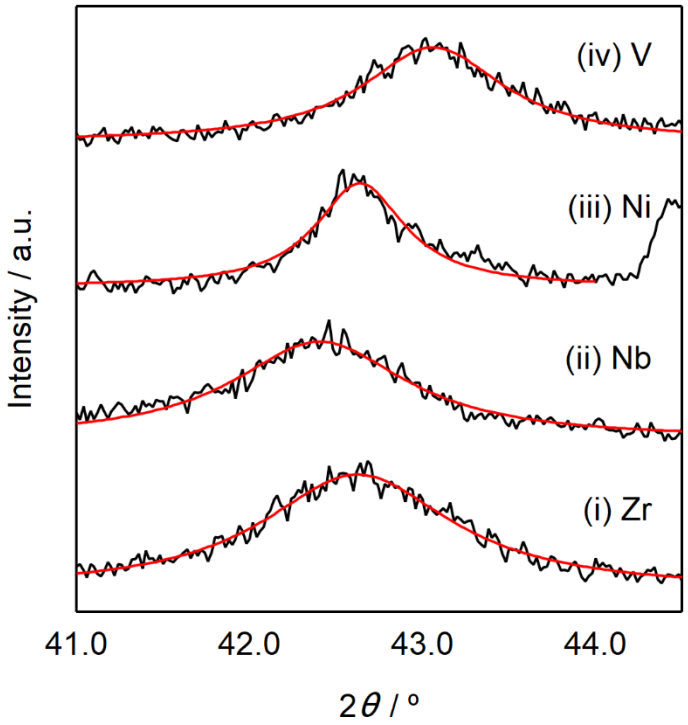

Fig. S3 X-ray diffraction (XRD) patterns at 2Θ = 41–44° of $Ti_{0.8}M_{0.2}O_xN_y$ catalysts, where M = (i) Zr,[S7] (ii) Nb, (iii) Ni and (iv) V.

S3. Morphology of $Ti_{0.8}Ni_{0.2}O_xN_y$ catalyst.

The dense morphology of $Ti_{0.8}Ni_{0.2}O_xN_y$ catalyst is observed from Fig. 2(iii), which is a secondary electron image. To investigate the surface roughness, the composition image, i.e., the backscattered electron image was obtained as shown in Fig. S4(A) because it is more sensitive to fine asperities when compared with a secondary electron image used to acquire Fig. 2. A small roughness is observed from the surface of $Ti_{0.8}Ni_{0.2}O_xN_y$ while it is fair to say that the surface is dense. It is noted that the magnification used to acquire Fig. S4 is ×11,000, which is more than 5 times higher than that for Fig. 2, ×2,000. Besides, many white bright spots are found in Fig. S4(A) which indicates the segregation of an element with the highest atomic number among the used chemicals for the synthesis of $Ti_{0.8}Ni_{0.2}O_xN_y$, Ni. Because both TiN and metallic nickel phases are observed from the XRD pattern of $Ti_{0.8}Ni_{0.2}O_xN_y$ shown in Fig. 1(a)-iii, the bright spots could be originated from metallic nickel particles. The energy dispersive X-ray spectroscopy (EDS) mapping results shown in Fig. S4(B)–(E) clearly indicates that both two elements, titanium and nickel evenly distributed over the area investigated. Thus, the dense morphology is mostly from aggregated TiN particles and smaller nickel particles are observed on the TiN surface. The nickel particles are not the source of ORR activity as discussed later in section S4.

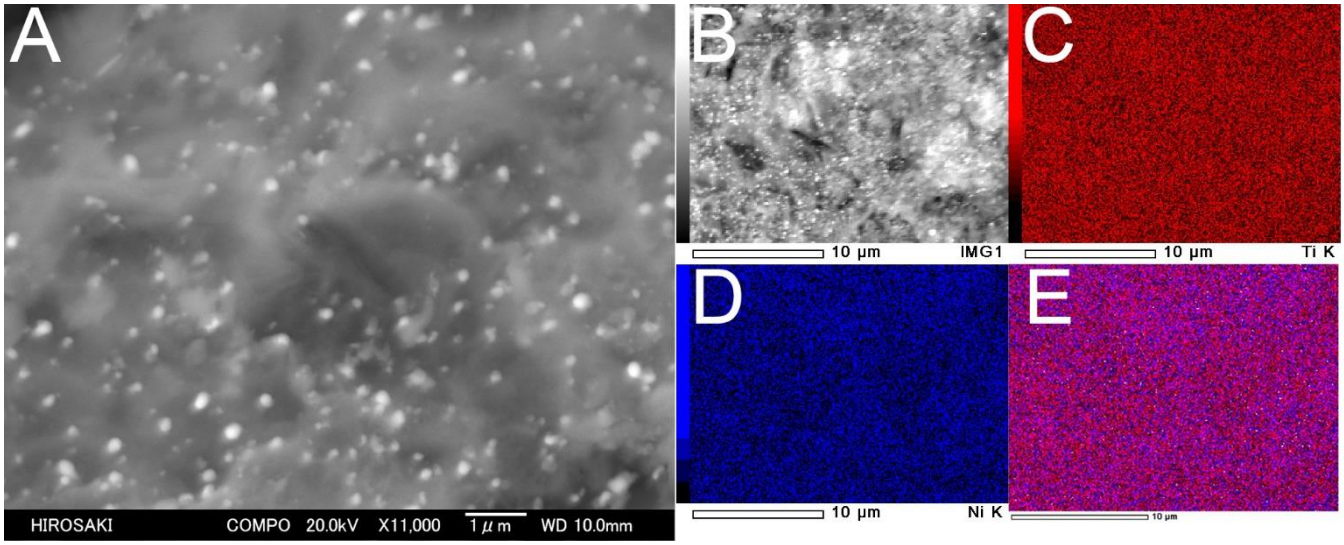

Fig. S4 A backscattered electron image of $Ti_{0.8}Ni_{0.2}O_xN_y$ catalyst at (A) high magnification and (B) low magnification. The energy dispersive X-ray spectroscopy (EDS) mapping images of (C) titanium, (D) nickel and (E) the overlapped image of (C) and (D). The EDS mappings (C)–(E) are performed on the sample area shown in (B).

S4. Stability of nickel metal in $Ti_{0.8}Ni_{0.2}O_xN_y$ catalyst during the electrochemical measurements.

To investigate the stability of metallic nickel in $Ti_{0.8}Ni_{0.2}O_xN_y$ during electrochemical measurements in 0.1 mol dm^{-3} H_2SO_4 solution, the catalyst powders with Nafion ionomer after the measurements were collected carefully from four different GC electrodes. The XRD patterns of $Ti_{0.8}Ni_{0.2}O_xN_y$ catalyst before and after the electrochemical (ORR) measurements are shown in Fig. S5. Both TiN and rutile TiO_2 phases survived whereas metallic nickel phase disappeared after the measurements. These results indicate that the metallic nickel dissolved into 0.1 mol dm^{-3} H_2SO_4 solution during the measurements, and the contribution of the metallic nickel to ORR activity of $Ti_{0.8}Ni_{0.2}O_xN_y$ catalyst shown in Fig. 3(A)-iii is ruled out.

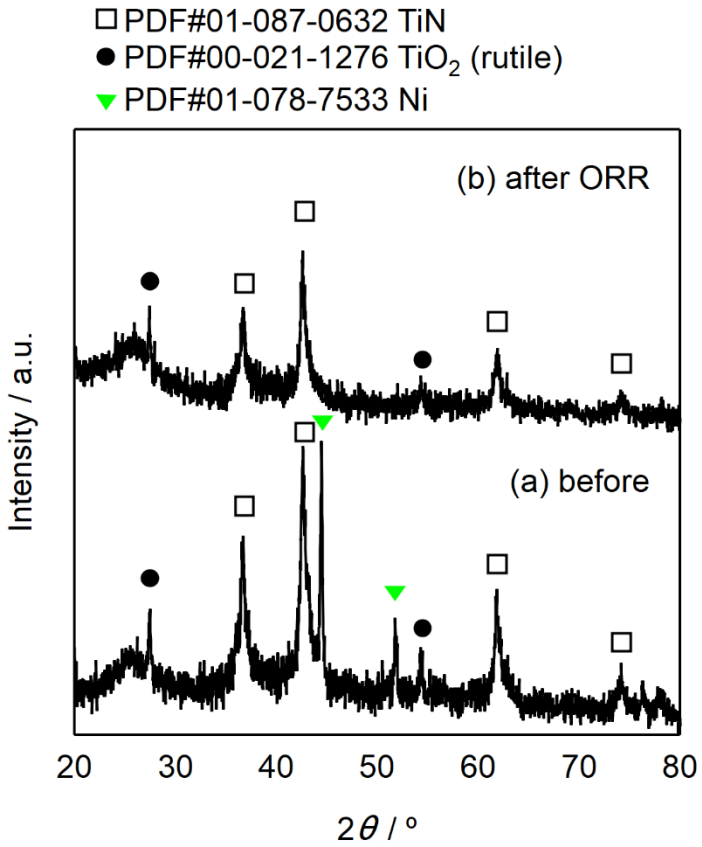

Fig. S5 XRD patterns of (a) as synthesised $Ti_{0.8}Ni_{0.2}O_xN_y$ catalyst before electrochemical (ORR) measurements and (b) $Ti_{0.8}Ni_{0.2}O_xN_y$ catalyst with Nafion ionomer after ORR measurements.

S5. The ORR mechanism on the $Ti_{0.8}M_{0.2}O_xN_y$ catalysts.

The four electron ($4e^-$) and two electron ($2e^-$) ORR in acidic media have been assumed to proceed *via* the several elementary steps shown in Fig. S6.[S8,S9]

$4e^-$ ORR

$$O_2 + 4H^+ + 4e^- \rightarrow 2H_2O \quad \text{(S4)}$$

$$O_2 + * \rightarrow O_2* \quad \text{(S4a)}$$

$$O_2* + H^+ + e^- \rightarrow HO_2* \quad \text{(S4b)}$$

$$HO_2* + H^+ + e^- \rightarrow H_2O + O* \quad \text{(S4c)}$$

$$O* + H^+ + e^- \rightarrow HO* \quad \text{(S4d)}$$

$$HO* + H^+ + e^- \rightarrow H_2O + * \quad \text{(S4e)}$$

$2e^-$ ORR

$$O_2 + 2H^+ + 2e^- \rightarrow H_2O_2 \quad \text{(S5)}$$

$$O_2 + * \rightarrow O_2* \quad \text{(S5a)}$$

$$O_2* + H^+ + e^- \rightarrow HO_2* \quad \text{(S5b)}$$

$$HO_2* + H^+ + e^- \rightarrow H_2O_2 + * \quad \text{(S5c)}$$

In both the $4e^-$ and $2e^-$ ORR processes, a peroxy intermediate, HO_2, is produced (S4b, S5b). Electron donating ability from the active site expressed by * and the strength of binding between HO_2 and * are key factors to determining *n*. However, oxide-based catalysts containing group IV or V metals have been investigated for only a short period of time, <20 years, and the ORR process has not been clarified. Rutile TiO_2 has been investigated as a catalyst for the oxygen evolution reaction (OER), which is the reverse reaction of the ORR. García-Mota *et al.* investigated the binding energy of HO_2 and * of the (1 1 0) plane

on various metal doped rutile TiO_2 catalysts using first principles density functional theory (DFT) calculations.[S10] Although zirconium was not included in their study, niobium, nickel and vanadium were investigated as dopants. The binding energy increased in the order of Nb < V < Ni.[S10] This trend is the reverse of *n* measured in this study, suggesting that strong *–HO_2 interactions inhibited the breaking of O–O bonding in the HO_2 intermediate to favour 2-electron ORR to produce H_2O_2.

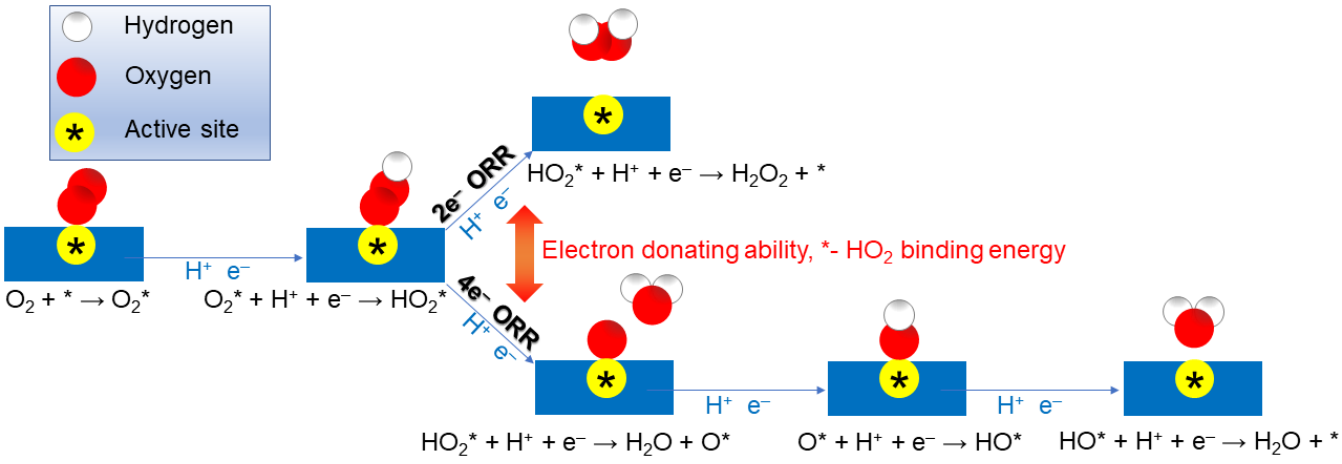

Fig. S6 Two reaction pathways for the oxygen reduction reaction (ORR) on conventional catalysts.

S6. Effect of niobium doping level on the ORR activity of the $Ti_{1-d}Nb_dO_xN_y$ catalysts and intrinsic activity analyses of $Ti_{1-d}M_dO_xN_y$ catalysts.

The niobium doping level, *d* of $Ti_{1-d}Nb_dO_xN_y$ catalysts were varied from 0.1 to 0.3 and the RDE voltammograms and XRD patterns are panelled in Fig. S7. The activity increases with increasing *d* from 0.1 to 0.2 whereas it deteriorates with increasing *d* further to 0.3 as shown in Fig. S7 (left). At the largest $d = 0.3$, the rutile TiO_2 content is the maximum among the three $Ti_{1-d}Nb_dO_xN_y$ catalysts as shown in Fig. S7 (right). These results indicate that doped niobium atoms created the active sites for ORR whereas they increased the content of rutile TiO_2 phase which is not conductive and thus to decrease the activity. Therefore, the activity of $Ti_{0.8}Nb_{0.2}O_xN_y$ displayed in Fig. 3(A)-ii is of the optimised composition.

To compensate for the effect of surface area on the activity of four $Ti_{0.8}M_{0.2}O_xN_y$ catalysts, the ORR current density shown in Fig. 3(A) is divided by the current density under N_2, $(j_O - j_N)\cdot j_N^{-1}$ as j_N is proportional to the surface area.[S11,S12] Then halfwave potential, $E_{1/2}$, i.e., the potential at which $(j_O - j_N)\cdot j_N^{-1}$ reached half of the maximum is obtained to evaluate the intrinsic activity which compensates for the magnitude of surface area. The $E_{1/2}$ values are 0.64, 0.62, 0.55 and 0.52 V when M is Zr, Nb, Ni and V, respectively. Therefore, the trend in j_k observed from Fig. 3(A) is not solely due to the surface area of catalysts.

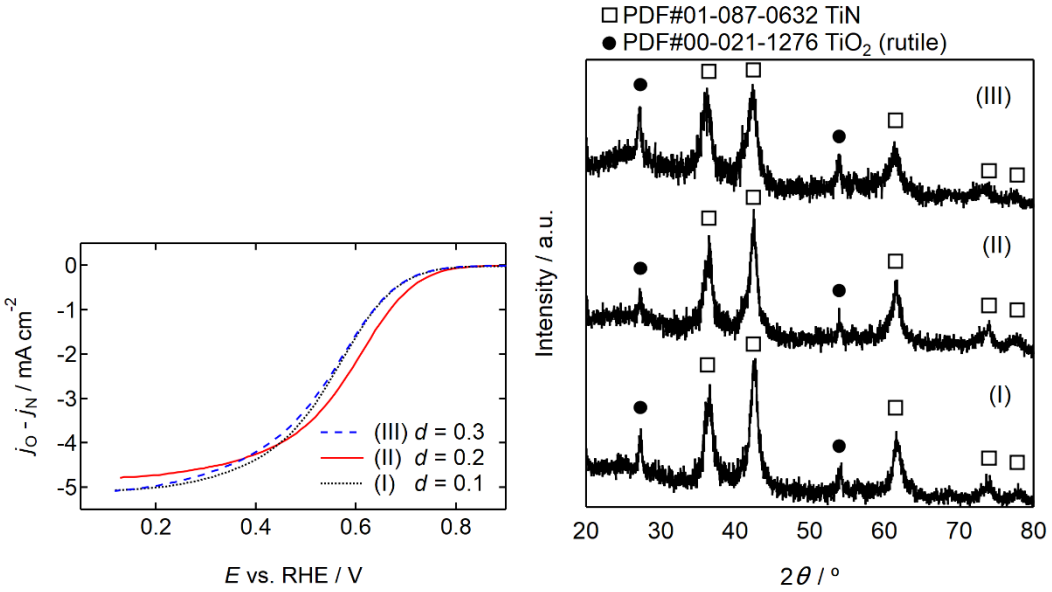

Fig. S7. (Left) Rotating disk electrode (RDE) voltammograms and (right) XRD patterns for $Ti_{1-d}Nb_dO_xN_y$ catalysts with three d values: (I) 0.1, (II) 0.2 and (III) 0.3.

Supplementary references

S1 M. Chisaka, Y. Ando, Yamamoto and N. Itagaki, *Electrochim. Acta*, 2016, **214**, 165.

S2 M. Chisaka, Y. Yamamoto, N. Itagaki and Y. Hattori, *ACS Appl. Energy Mater.*, 2018, **1**, 211.

S3 K. S. Robinson and M. A. Sherwood, *Sur. Interface Anal.*, 1984, **6**, 261.

S4 Y. Cong, J. Zhang, F. Chen and M. Anpo, *J. Phys. Chem. C*, 2007, **111**, 6976.

S5 A. Rizzo, M. A. Signore, L. Mirenghi and T. Di Luccio, *Thin Solid Films*, 2009, **517**, 5956.

S6 H. B. Michaelson, *J. Appl. Phys.*, 1977, **48**, 4729; J. R. Rumble in CRC Handbook of Chemistry and Physics, 103rd ed., CRC Press, FL, 2022, p. 12-114.

S7 M. Chisaka, R. Xiang, S. Maruyama and H. Daiguji, *Energy Fuels*, 2022, **36**, 539.

S8 J. K. Nørskov, J. Rossmeisl, A. Logadottir, L. Lindqvist, J. R. Kitchin, T. Bligaard and H. Jónsson, *J. Phys. Chem. B*, 2004, **108**, 17886.

S9 S. Siahrostami, S. J. Villegas, A. H. B. Mostaghimi, S. Back, A. B. Farimani, H. Wang, K. A. Persson, and J. Montoya, *ACS Catal.*, 2020, **10**, 7495.

S10 M. García-Mota, A. Vojvodic, H. Metiu, I. C. Man, H. Y. Su, J. Rossmeisl and J. K. Nørskov, *ChemCatChem*, 2011, **3**, 1607.

S11 A. Ishihara, S. Doi, S. Mitsushima and K. Ota, *Electrochim. Acta*, 2008, **53**, 5442.

S12 M. Chisaka, T. Iijima, A. Tomita, T. Yaguchi and Y. Sakurai, *J. Electrochem. Soc.*, 2010, **157**, B1701.